Cell Reports

TCF/LEF regulation of the topologically associated domain *ADI* promotes mESCs to exit the pluripotent ground state

Graphical abstract

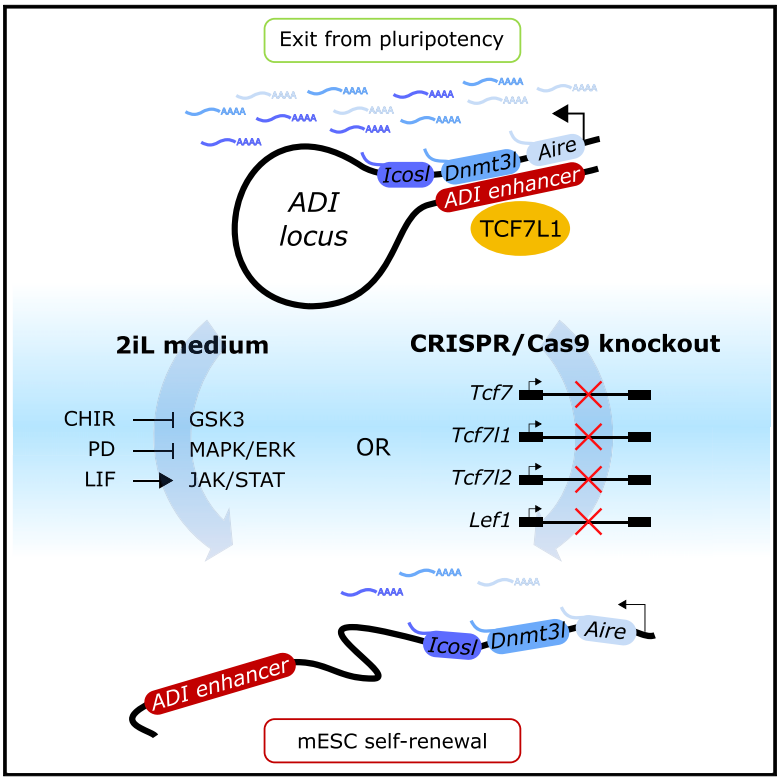

Highlights

- Generation of TCF/LEF-KO, β-catenin-KO, and TCF/LEF+β-catenin-KO mESC lines
- Quadruple TCF/LEF-KO (qKO) mESCs self-renew in the absence of 2iL
- *Aire*, *Dnmt3l*, and *IcosL* are targets of TCF/LEF but not of β-catenin
- *Aire* and *Dnmt3l* are functional TCF/LEF effectors mediating the exit from pluripotency

Authors

Nikolaos Doumpas, Simon Söderholm, Smarth Narula, Steven Moreira, Bradley W. Doble, Claudio Cantù, Konrad Basler

Correspondence

claudio.cantu@liu.se (C.C.), konrad.basler@imls.uzh.ch (K.B.)

In brief

Doumpas et al. show that mESCs with genetic deletion of all four TCF/LEF transcription factors self-renew in the absence of GSK and MEK inhibition. TCF/LEFs drive mESCs to exit their state of self-renewal through Wnt/b-catenin-independent transcriptional regulation of the ADI domain that contains three genes, *Aire*, *Dnmt3l*, and *IcosL*.

Doumpas et al., 2021, Cell Reports *36*, 109705
September 14, 2021
https://doi.org/10.1016/j.celrep.2021.109705

Cell Reports

CellPress
OPEN ACCESS

Report

TCF/LEF regulation of the topologically associated domain *Adi* promotes mESCs to exit the pluripotent ground state

Nikolaos Doumpas,[1,6] Simon Söderholm,[2,3,6] Smarth Narula,[4] Steven Moreira,[4] Bradley W. Doble,[4,5] Claudio Cantù,[2,3,7,8,*] and Konrad Basler[1,7,*]

[1]Department of Molecular Life Sciences, University of Zurich, Zurich, Switzerland
[2]Wallenberg Centre for Molecular Medicine, Linköping University, Linköping, Sweden
[3]Department of Biomedical and Clinical Sciences, Division of Molecular Medicine and Virology, Faculty of Medicine and Health Sciences, Linköping University, Linköping, Sweden
[4]Department of Biochemistry and Biomedical Sciences, McMaster University, Hamilton, ON L8N 3Z5, Canada
[5]Departments of Biochemistry and Medical Genetics & Pediatrics and Child Health, University of Manitoba, Winnipeg, MB R3E 0W2, Canada
[6]These authors contributed equally
[7]Senior author
[8]Lead contact
*Correspondence: claudio.cantu@liu.se (C.C.), konrad.basler@imls.uzh.ch (K.B.)
https://doi.org/10.1016/j.celrep.2021.109705

SUMMARY

Mouse embryonic stem cells (mESCs) can be maintained *in vitro* in defined N2B27 medium supplemented with two chemical inhibitors for GSK3 and MEK (2i) and the cytokine leukemia inhibitory factor (LIF), which act synergistically to promote self-renewal and pluripotency. Here, we find that genetic deletion of the four genes encoding the TCF/LEF transcription factors confers mESCs with the ability to self-renew in N2B27 medium alone. TCF/LEF quadruple knockout (qKO) mESCs display dysregulation of several genes, including *Aire*, *Dnmt3l*, and *IcosL*, located adjacent to each other within a topologically associated domain (TAD). *Aire*, *Dnmt3l*, and *IcosL* appear to be regulated by TCF/LEF in a β-catenin independent manner. Moreover, downregulation of *Aire* and *Dnmt3l* in wild-type mESCs mimics the loss of TCF/LEF and increases mESC survival in the absence of 2iL. Hence, this study identifies TCF/LEF effectors that mediate exit from the pluripotent state.

INTRODUCTION

Mouse embryonic stem cells (mESCs) are derived from pre-implantation blastocyst cells that, when cultured *in vitro*, display unrestrained self-renewal while preserving differentiation potential (Huang et al., 2015; Evans and Kaufman, 1981). mESCs can be propagated in a chemically defined medium termed N2B27, supplemented with two specific inhibitors (2i) to secure pluripotency: CHIR99021 (hereafter referred to as CHIR) inhibits glycogen synthase kinase 3 (GSK3), and PD0325901 (referred to as PD) blocks mitogen-activated protein kinase kinase (MEK, also known as MAPKK) (Ying et al., 2008). Further addition of LIF (leukemia inhibitory factor) activates JAK/STAT3 signaling to stimulate self-renewal (Smith et al., 1988). "2iL" in N2B27 is the standard cocktail to allow mESCs to divide perpetually, to preserve the features of the inner cell mass of the blastocyst (Blair et al., 2011; Morgani et al., 2017), and to sustain stable expression of the transcription factors typical of the naive pluripotency gene regulatory network (Blair et al., 2011; Dunn et al., 2014; Morgani et al., 2017; Mulas et al., 2019).

Many efforts have been devoted to identify genes that promote exit from the pluripotent state and the transition to a primed state of differentiation (Betschinger et al., 2013; Guo et al., 2011; Kinoshita et al., 2020; Li et al., 2018; Villegas et al., 2019). The Wnt/β-catenin effector TCF7L1 (previously referred to as TCF3), belonging to the family of four TCF/LEF transcription factors, was one of the first identified players in this process (Pereira et al., 2006). Mechanistically, TCF7L1 acts as pro-differentiation factor by repressing pluripotency genes such as *Nanog* and *Klf2* (Dunn et al., 2014; Pereira et al., 2006; Yeo et al., 2014), and its activity is counteracted by CHIR-mediated GSK3 inhibition (Martello et al., 2012; Qiu et al., 2015). CHIR stabilizes β-catenin that, in turn, is thought to abrogate TCF7L1 repression of pluripotency genes thereby allowing a Wnt signaling response mediated by other TCF/LEF factors (Wray et al., 2011; Yi et al., 2011). Hence, it has been hypothesized that β-catenin stabilization is a key mechanism by which CHIR promotes mESC self-renewal (Aulicino et al., 2020; Kelly et al., 2011; Wray et al., 2011; Yi et al., 2011). On the other hand, β-catenin stabilization could induce the activation of differentiation genes upon interaction with TCF7 and LEF1 (Chatterjee et al., 2015; Chen et al., 2013), indicating that fine-tuning of this pathway is crucial for the balance between self-renewal and differentiation of mESCs (Habib et al., 2013).

Of note, there is little evidence that the genetic abrogation of the mechanisms required for the exit from the pluripotent state

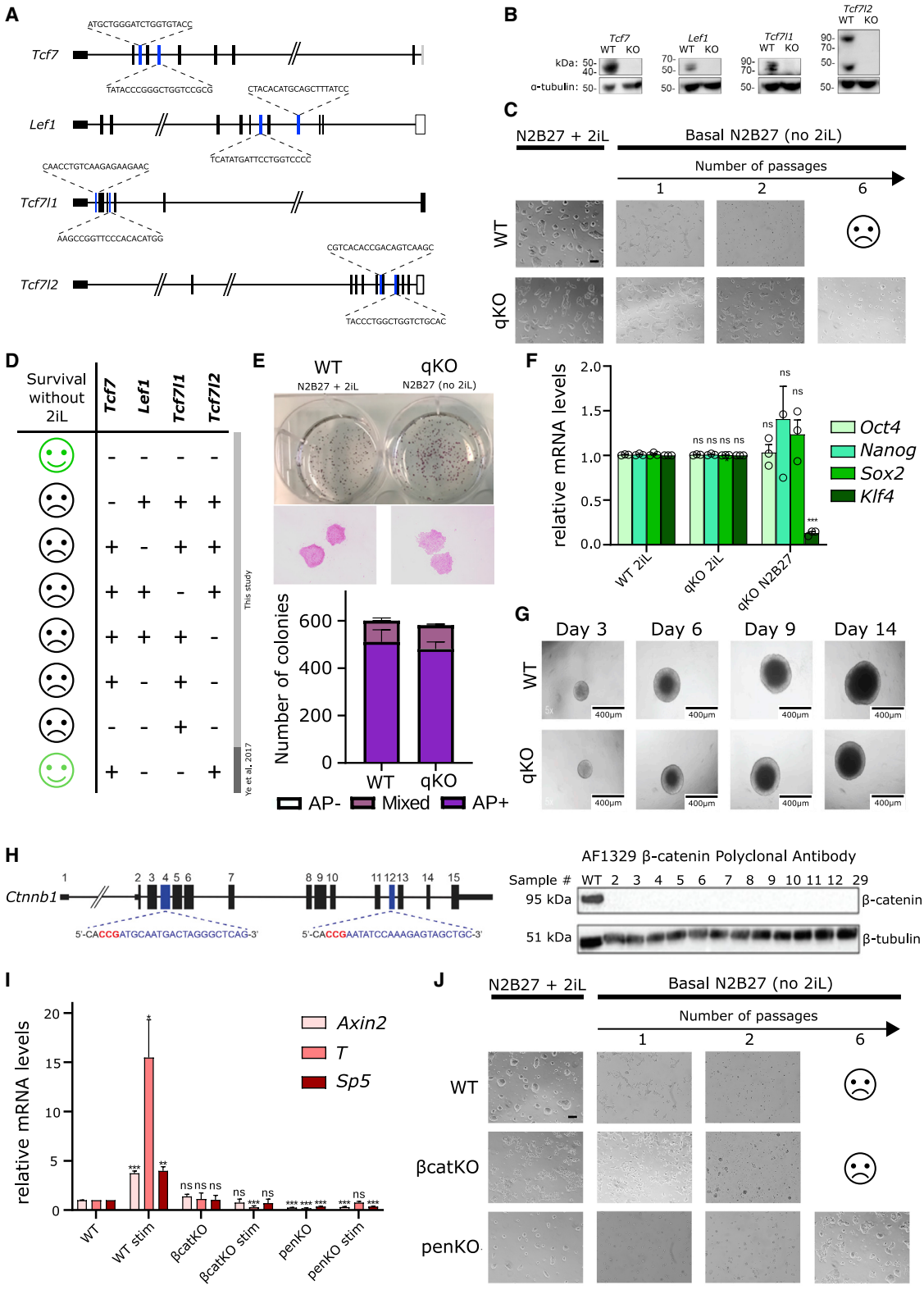

(legend on next page)

is sufficient to enable self-renewal in the absence of 2iL (Guo et al., 2011; Wray et al., 2011). For example, homozygous *Tcf7l1* deletion confers enhanced self-renewal but does not substitute for LIF (Guo et al., 2011). Recent efforts identified a number of factors that contribute to the transition from pluripotency to differentiation, such as the transcription factor ETV5 (Kalkan et al., 2019), or the plasma membrane Ca^{2+} pump ATP2b1 (MacDougall et al., 2019). Loss-of-function mutations of *Etv5* or *Atp2b1*, when introduced in a *Tcf7l1* knockout background, allow maintenance of mESC self-renewal in the absence of 2iL.

Here, we found that complete loss-of-function of *Tcf7*, *Lef1*, *Tcf7l1*, and *Tcf7l2*, the genes encoding for the four TCF/LEF transcription factors, allows mESCs to become fully 2iL-independent and to propagate in basal N2B27 *ad libitum*. Transcriptomics profiles (RNA sequencing [RNA-seq]) and chromatin immunoprecipitation (ChIP-seq) data pointed to a TCF/LEF-regulated locus containing three genes, *Aire*, *Dnmt3l*, and *IcosL*. These genes are clustered within a topologically associated domain (TAD), and their downregulation functionally contributes to the acquired 2iL-independent self-renewal. Importantly, this mechanism appears to be independent of β-catenin, thus suggesting that an alternative TCF/LEF-dependent regulatory mechanism is employed at this locus.

RESULTS

We generated quadruple knockout (qKO) mESCs bearing loss-of-function mutations in the four genes encoding the TCF/LEF family of transcription factors (Figure 1A). qKO mESCs did not display any detectable TCF/LEF protein (Figure 1B) and were incapable of transducing Wnt/β-catenin-dependent transcription upon pathway stimulation (Figure S1). Surprisingly, qKO cells acquired the ability to proliferate in N2B27 basal medium without 2iL supplement, a condition in which wild-type mESCs (WT) are lost after only a maximum of two passages (Morgani et al., 2017) (Figure 1C). Systematic testing of cell lines carrying different combinations of TCF/LEF knockouts revealed that survival in the absence of 2iL is possible only when all *Tcf./Lef* genes are nullizygous (Figure 1D). Of note, a recent report provided evidence that compound deletion of only *Tcf7l1* and *Lef1* induced similar 2iL-independent renewal properties (Ye et al., 2017). Combined with our observation, this suggests that TCF/LEF proteins possess non-redundant functions in mESCs, and that TCF7L1 and LEF1 likely represent the key effectors that induce the exit from the pluripotent state.

To test whether qKO mESCs maintained stem cell features in the absence of 2iL—in addition to cell proliferation—we exploited three classic approaches. First, we performed staining for alkaline phosphatase (AP), a key marker of pluripotency in ESCs (Štefková et al., 2015). 6 days after single-cell plating in basal N2B27, qKO cells remained AP positive and were undistinguishable from WT colonies grown in 2iL medium, both in shape and number (Figure 1E). Second, we measured the expression of the pluripotency genes, *Oct4*, *Nanog*, *Sox2*, and *Klf4* via quantitative reverse transcriptase PCR (qRT-PCR). Even after 14 days in basal N2B27 medium, qKO mESCs still expressed levels of *Oct4*, *Nanog*, and *Sox2* comparable to WT control cells grown in presence of 2iL (Figure 1F). *Klf4* expression was decreased, suggesting possible alternative regulation of this gene, which did not perturb self-renewal. Finally, we allowed spontaneous differentiation into embryoid bodies (EBs), embryo-like aggregates containing cells of all three germ layer lineages (Doetschman et al., 1985). qKO cells formed EBs that expressed general differentiation markers similarly to those derived from WT cells, showing that deletion of TCF/LEF does not prohibit exit from pluripotency (Figure 1G).

While TCFL1 is known to repress pluripotency genes (Dunn et al., 2014), TCF7 was shown to promote mESC differentiation in a β-catenin-dependent manner (Chatterjee et al., 2015). It is

Figure 1. qKO mESCs display 2iL-independent self-renewal

(A) Schematic representation of the genetic loci encoding the TCF/LEF transcription factors. Annotated in blue are the gRNA sequences and target coding regions.

(B) Western blots for detection of TCF7, LEF1, TCF7L1, and TCF7L2, in parental (WT) and qKO mutant mESCs.

(C) Wild-type (WT) and qKO mESCs were cultured for 6 passages (a total of 14 days) in N2B27 lacking 2iL. WT cells, which survive in N2B27+2iL (left panels) are lost after 2 passages in the absence of 2iL. qKO divide indefinitely in this condition. The black scale bar displayed on the top-left image represents approximately 200 μm.

(D) mESCs bearing different combinations of mutations in TCF/LEF genes were tested for survival in basal N2B27 medium (no 2iL). In the table, presence or absence of a particular factor is indicated by a "+" or a "–," respectively. Clonal lines that perpetuate in absence of 2iL are indicated by a happy green smile, in this case for the quadruple knockout, while those that do not survive after 2 passages are indicated by a black sad smile.

(E) Clonogenicity assay based on alkaline phosphatase (AP) positivity. Top pictures, whole plate image. Bottom pictures, single-cell resolution image. Bottom panel, quantification of colonies: AP^- (white cells) differentiated, mix (light purple cells) differentiated and un-differentiated, AP^+ (purple cells) un-differentiated. WT cells were cultured in the presence of 2iL while the qKO cells were culturing without 2iL. The data represent the mean ± SEM obtained from three independent experiments (n = 3). Samples were compared using Student's t test. *$p < 0.05$.

(F) qRT-PCR analysis of *Oct4*, *Nanog*, *Sox2*, and *Klf4* transcripts, performed on WT and qKO mESCs, cultured in N2B27 medium with or without 2iL. The data represent the mean ± SEM obtained from three independent experiments (n = 3). Samples were compared using Student's t test. ***$p < 0.001$; ns, not significant ($p > 0.05$).

(G) WT and qKO mESCs formed superficially similar embryoid bodies (EBs) using the hanging drop technique for a total of 14 days. EBs were imaged at days 3, 6, 9, and 14.

(H) Schematic representation of the *Ctnnb1* gene. Annotated with blue are the gRNA sequences and targeted regions. Right panel: western blot for detection of β-catenin in WT and several gRNA-treated clones.

(I) WT, β-catenin knockout (βcatKO), and TCF/LEF+β-catenin knockout (penKO) clones were evaluated for their ability to express specific Wnt signaling target genes (*Axin2*, *T*, *Sp5*) after 24 h stimulation with 10 μM CHIR. The data represent the mean ± SEM obtained from three independent experiments (n = 3). Samples were compared using Student's t test. *$p < 0.05$; **$p < 0.01$; ***$p < 0.001$; ns, not significant ($p > 0.05$).

(J) WT, βcatKO, and penKO cells were cultured for 6 passages (a total of 14 days) in N2B27 lacking 2iL. As with WT cells, βcatKO survive in N2B27+2iL (left panels) but are lost after 2 passages in the absence of 2iL. penKO divide indefinitely in this condition. The black scale bar displayed on the top-left image represents approximately 200 μm.

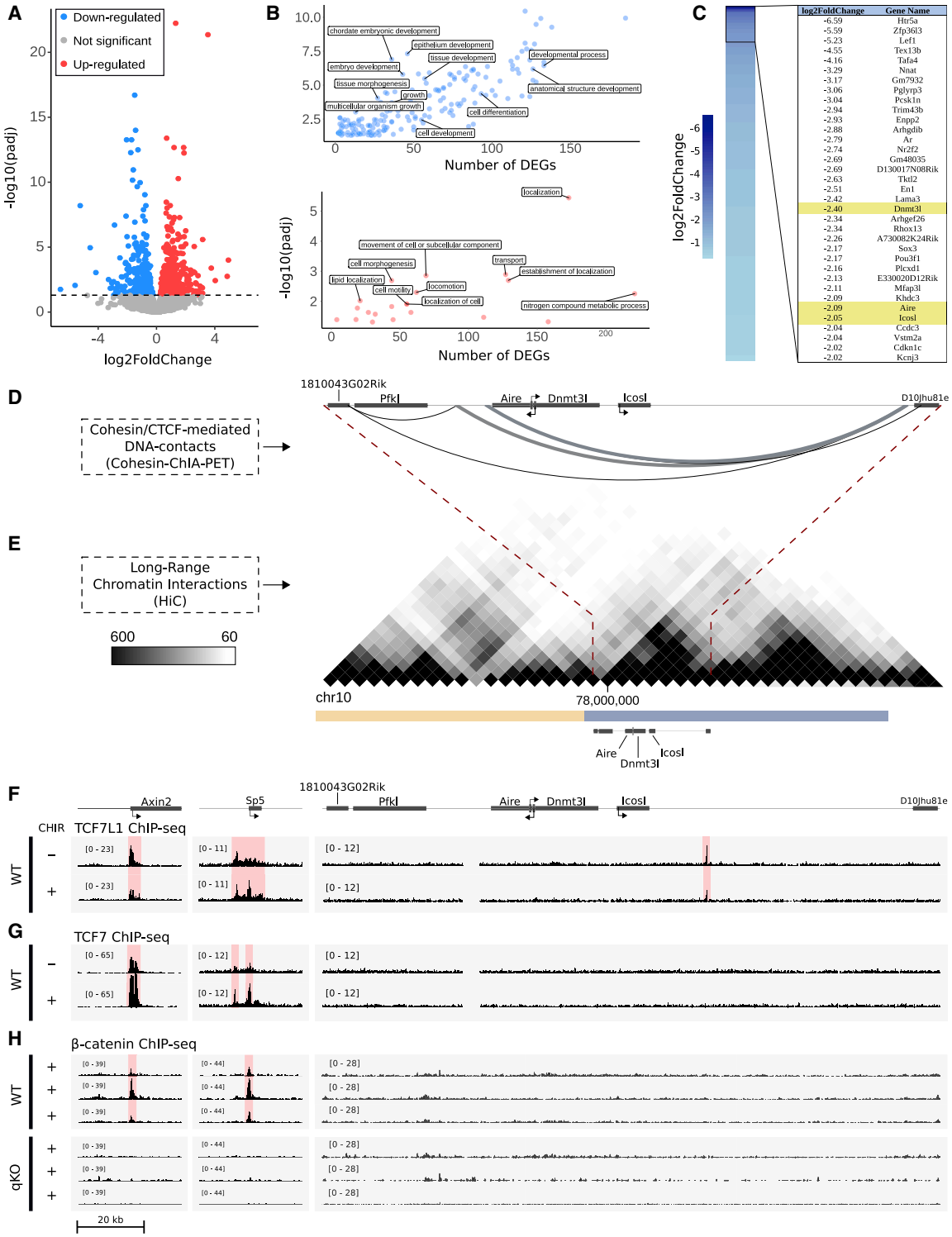

Figure 2. *Aire*, *Dnmt3l*, and *IcosL* are TCF/LEF effectors

(A) Volcano plot of differentially expressed genes (DEGs) in the qKO versus WT comparison (without additional CHIR stimulation). The x axis shows logarithmically (log2) transformed fold change of expression, while the y axis represents the –log10-transformed FDR-adjusted p values. Each dot represents an individual gene. Blue dots correspond to downregulated genes and red dots to upregulated genes. Gray dots denote genes whose differential expression was not statistically significant based on an FDR-adjusted p value threshold of 0.05.

(legend continued on next page)

plausible that the mere inability of activating canonical Wnt/β-catenin signaling locks qKO cells in a perpetual self-renewing state. We tested this by inducing loss-of-function mutations in *Ctnnb1*, the gene encoding for β-catenin, both in WT mESCs (to obtain β-catenin knockout, βcatKO cells), and in qKO cells (to obtain penta-knockout, penKO cells). The use of guide RNA (gRNA) targeting exons 4 and 12 resulted in several clones displaying loss of detectable β-catenin protein (Figure 1H). As expected, βcatKO and penKO clones were incapable of activating Wnt-dependent transcription, as seen by their failure to induce endogenous Wnt target gene expression upon CHIR stimulation (Figure 1I). However, βcatKO cells could not propagate in the absence of 2iL, while penKO behaved in a manner indistinguishable from qKO (Figure 1J; Figure S2). Note that this experiment, while not informative regarding the role of β-catenin in mESC cell differentiation (Chatterjee et al., 2015; Lyashenko et al., 2011), demonstrates that blocking the output of TCF/LEF-mediated Wnt/β-catenin signaling is not sufficient to allow 2iL-independent mESC self-renewal.

To understand the genetic changes that follow deletion of TCF/LEF and might allow qKO cells to achieve 2iL-independent self-renewal, we performed RNA-seq of qKO and WT mESCs cultured in standard 2iL and identified 512 upregulated and 348 downregulated genes in qKO cells (Figure 2A; Figures S3A and S3B; Table S1). In agreement with previous data (Moreira et al., 2017), qKO cells had reduced expression of endoderm and mesoderm markers (Figure S3B). Gene Ontology (GO) scrutiny revealed that genes involved in embryonic development and cell differentiation were enriched among the downregulated groups (Figure 2B). In particular, we noticed that close to the top of the list of genes ranked based on their fold change, three displayed similar levels of downregulation and encode: autoimmune regulator (*Aire*), DNA methyltransferase 3 like (*Dnmt3l*), and inducible T cell co-stimulator ligand (*IcosL*) (Figure 2C; Figure S3C). Surprisingly, these genes are located adjacent to each other within the same genomic locus at 10qC1 (Figure 2D), and their chromosomal arrangement is conserved between mouse and human. By exploring Cohesin-ChIA-PET datasets obtained from mESC studies (Dowen et al., 2014), we found that the genomic borders of this locus are marked by Cohesin complexes, likely representing the boundaries of a topologically associated domain (TAD, Dixon et al., 2012) (Figure 2D), to which we refer as the *ADI* locus (for *Aire-Dnmt3l-IcosL*). Intriguingly, the *ADI* locus displays a high frequency of DNA-DNA interactions in mESCs, as indicated by Hi-C experiments, and has been previously annotated as a subdomain within a TAD (Figure 2E; Bonev et al., 2017).

We hypothesized that TCF/LEF family members could contribute to the regulation of the genes in the *ADI* locus and used chromatin immunoprecipitation followed by deep DNA sequencing (chromatin immunoprecipitation sequencing [ChIP-seq]) to assess potential physical association of these transcription factors with this locus. We identified TCF7L1 ChIP-seq peaks in the proximity of several genes differentially expressed in qKO cells, including one at the center of the *ADI* locus, downstream of the *IcosL* coding sequence (Figure 2F; Table S2; Moreira et al., 2018). The size of the TCF7L1 ChIP-seq peak at this location was present but slightly reduced upon increase of CHIR concentration (Figure 2F, bottom track). Of note, the observed reduction in peak intensity is likely due to a CHIR-induced decrease in TCF7L1 protein levels (Figure S3D), corroborating previous reports showing that CHIR causes *Tcf7l1* downregulation in mESCs (Ye et al., 2017). TCF7, which did not confer dependency on 2iL, showed no association with this locus (Figure 2G). Consistent with our genetic evidence, no β-catenin ChIP-seq peak was ever detected within the borders of the *ADI* locus across three independent experiments in CHIR-stimulated mESCs. (Figure 2H). On the other hand, β-catenin association was always observed at classic Wnt responsive elements (WREs) present in the *Axin2* and *Sp5* promoters, where it requires TCF/LEF for its physical association with DNA targets (Figure 2H; Figure S4; Table S3).

Notably, this TCF7L1-bound DNA region has been previously annotated as a typical enhancer in mESCs (Figure 3A; Dowen et al., 2014), and it also displayed simultaneous presence of H3K4me1 and H3K27ac histone marks (Figure 3A; Joshi et al., 2015); we refer to this regulatory region as the *ADI* enhancer. To test whether the *ADI* enhancer is responsive to TCF7L1, we PCR-amplified the genomic region of ~200 bp underlying the

(B) Functional enrichment analysis of differentially expressed genes (DEGs) in the qKO versus WT comparison (without additional CHIR stimulation), based on the Gene Ontology (GO) knowledgebase. Significantly enriched biological pathways were assessed based on an FDR-adjusted p value of 0.05. Each dot represents a significantly enriched pathway. The x axis shows number of DEGs found to be annotated for each pathway, and the y axis shows –log10-transformed FDR-adjusted p values. Top panel: downregulated DEGs enriched for 342 GO terms. Enriched biological pathways related to processes such as development and cell differentiation are indicated with labels. Bottom panel: upregulated DEGs enriched for 33 GO-terms. Here, the top 10 pathways have been indicated with labels.
(C) Downregulated DEGs in the qKO versus WT comparison sorted by log2FoldChange. Among the top 35 downregulated DEGs we noticed three genes (*Aire*, *Dnmt3l*, and *IcosL*) for which subsequent analyses were focused on.
(D) Cohesin/CTCF-mediated chromatin interactions obtained by ChIA-PET (Dowen et al., 2014) are detected occurring within the genomic locus in chromosome 10 that contains *Aire*, *Dnmt3l*, and *IcosL*. Regions presenting statistically increased DNA-DNA interactions are indicated by dark-gray arches. Thick arches suggest that the *ADI* locus might be part of a topologically associate domain (TAD).
(E) Chromatin interaction heat map of Hi-C data from Bonev et al. (2017) at 25 kb resolution. Alternating yellow and blue bars indicate predicted topologically associated domains (TADs) Enrichment of long-range chromatin interactions are spanning a region containing the *ADI* locus and the potential TCF7L1 binding site. This interaction-rich region has been identified as part of a larger TAD. The heat map was created using the 3D Genome Browser.
(F) Top: schematic representation of genomic regions focused on the promoter of the genes *Axin2* and *Sp5* which contain classic Wnt responsive elements (WRE) required for TCF/LEF binding, and the genomic region housing the *Aire*, *Dnmt3l*, and *Icosl* genes (*ADI*). Below: genomic tracks showing TCF7L1 ChIP-seq peaks at the different loci. Peaks are emphasized by semi-transparent red boxes.
(G) Genomic tracks as shown in (D) for TCF7 ChIP-seq peaks. Peaks are scored at the *Axin2* and *Sp5* WRE but not within the *ADI* locus.
(H) Genomic tracks as shown in (D) and (E) for β-catenin ChIP-seq peaks. Peaks are scored at the *Axin2* and *Sp5* WRE but not within the *ADI* locus. Three independent replicates of β-catenin ChIP-seq are presented, and their reliability is additionally corroborated by the loss of β-catenin peaks on classic WRE in qKO (bottom tracks).

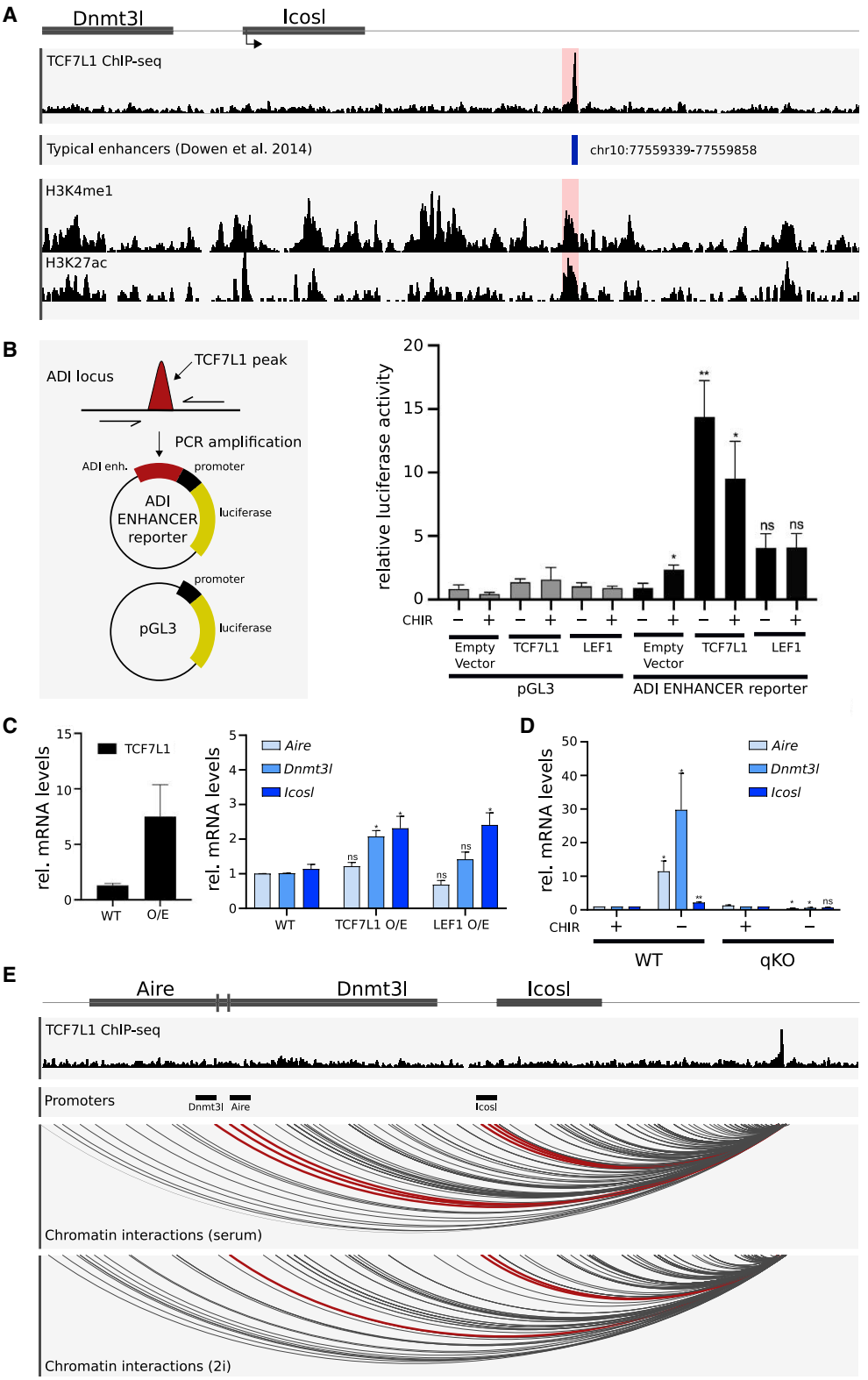

(legend on next page)

TCF7L1 ChIP-seq peak and cloned it into a Luciferase expression plasmid upstream of a minimal *thymidine kinase* gene promoter (Figure 3B). Remarkably, TCF7L1 overexpression produced an ~ 15-fold activation of the *ADI* enhancer reporter, while it did not induce any transcriptional activity of the minimal promoter control reporter (Figure 3B, right). In agreement with our previous observation that CHIR induced a mild TCF7L1 downregulation, CHIR quantitatively, but not completely, decreased the induction of the *ADI* enhancer by TCF7L1 (Figure 3B). Of note, overexpression of TCF7L1 in HEK293T cells induced a significant upregulation of *Aire*, *Dnm3tl*, and *IcosL* (Figure 3C), supporting the notion of a direct transcriptional regulation of the genes in the *ADI* locus by TCF7L1. The ability of TCF7L1 to induce transcription *in vitro* from the *ADI* enhancer raised the prediction that removal of CHIR from the culture medium would allow TCF7L1 to activate the *ADI* genes in mESCs. Indeed, we found that the expression of the *ADI* genes is suppressed by CHIR, while removing CHIR from the culture medium, a condition that still allows mESCs to divide, results in significant transcriptional upregulation of the *ADI* genes (Figure 3D). This regulation is dependent on TCF/LEF, as the upregulation of the *ADI* genes did not occur in qKO cells (Figure 3D). Notably, we detected significant upregulation of *Aire* also in βcatKO cells upon CHIR removal (as it occurs in WT cells), while *Dnmt3l* and *IcosL* remained unchanged (Figure S3E); this indicates that the CHIR-mediated, TCF7L1-dependent regulation of *Aire* is likely β-catenin independent. To further test the notion that the *ADI* enhancer regulates the expression of *Aire*, *Dnmt3l*, and *Icosl*, we analyzed the Capture Hi-C data from Joshi and colleagues, which recorded the DNA-DNA interactions occurring in mESCs with high resolution (Joshi et al., 2015), and focused on the *ADI* locus. When mESCs are cultured in DMEM containing 10% fetal calf serum and LIF, the *ADI* enhancer displays several long-range chromatin contacts within this locus, including significant ones with the promoters and coding sequences of *Aire*, *Dnmt3l*, and *Icosl* (Figure 3E). Consistent with our observations, these interactions appear to be decreased when 2i is added to the culture medium (Figure 3E), supporting the notion that CHIR inhibits the functional association between *Aire*, *Dnmt3l*, and *Icosl* and the *ADI* enhancer.

Our observations raise the possibility that *ADI* genes are relevant TCF/LEF targets that induce the exit from the pluripotent state. Therefore, we tested whether their decreased expression in qKO could contribute to the sustained 2iL-independent self-renewal. We induced downregulation of the *ADI* genes expression in WT mESCs and assessed the capability of treated cells to divide in 2iL-deprived N2B27 basal medium (Figure 4A). By means of small interfering RNAs (siRNAs), we achieved efficient and relatively stable downregulation of *Aire* and *Dnmt3l* and, albeit to a lesser extent, of *IcosL* (Figure 4B). WT mESCs electroporated with scrambled siRNAs could not divide in basal N2B27 and died after 4 days (Figure 4C). Notably, simultaneous downregulation of the *ADI* genes extended cell self-renewal over 7 days of culture (Figure 4C). Strikingly, individual downregulation of *Aire* or *Dnmt3l* had a similar effect on colony viability (Figure 4C), suggesting that these two genes might contribute to the balance between self-renewal and differentiation via parallel, non-redundant mechanisms. In addition to the proliferation/viability assay, we tested the expression of the pluripotency genes *Oct4*, *Nanog*, *Sox2*, and *Klf4*. Depletion of 2iL, in WT cells, caused loss of self-renewal accompanied by a drop in the expression of these genes (Figure 4D). Consistent with their sustained ability to divide, and similarly to qKO cells, mESCs with decreased expression of *Aire, Dnmt3l*, and *IcosL* maintained high expression of the pluripotency transcription factors to levels comparable to WT cells (Figure 4D). Taken together, these data support a model in which decreased expression of the genes in the *ADI* locus in qKO cells is responsible, at least in part, for the acquired independence of the 2iL inhibitors.

DISCUSSION

Here, we report the surprising observation that the loss of all TCF/LEF transcription factors confers to mESCs the ability to self-renew in the absence of CHIR, PD, and LIF. This effect is likely achieved through downregulation of three key genes physically located within the same genomic locus: *Aire*, *Dnmt3l*, and *IcosL*. These genes belong to a TAD, suggesting that they are co-regulated in mESCs. In particular, *Aire* and *Dnmt3l* have overlapping, yet directionally opposing transcriptional start sites, hinting

Figure 3. TCF7L1 binds enhancer in a TAD influencing *ADI* gene expression

(A) Genomic tracks with focus on the TCF7L1 binding site downstream of the *ADI* locus. First track: TCF7L1 ChIP-seq showing the binding peak emphasized by a semi-transparent red box. Second track: typical enhancers predicted by Dowen et al. (2014). One such enhancer region is seen overlapping the TCF7L1 peak within the *ADI* locus. Third and fourth tracks: histone modifications (H3K4me1 and H3K27ac, respectively) from Joshi et al. (2015). The histone modification peaks overlapping the TCF7L1 binding site have been emphasized by semi-transparent red boxes and further support the notion that this site has regulatory properties.

(B) Left panel: schematic representation of the TCFL7L1 enhancer peak tested in a luciferase assay (*ADI* enhancer reporter). Right panel: *ADI* enhancer reporter response in different stimulation conditions: +/− CHIR, +/− TCF7L1 or LEF1 overexpression. Samples were compared using Student's t test. *$p < 0.05$; **$p < 0.01$; ns, not significant ($p > 0.05$).

(C) Left panel: qPCR validation of TCF7L1 overexpression in HEK293T. Right panel: expression of the *ADI* genes was measured via qRT-PCR upon overexpression of TCF7L1 or LEF1. The data represent the mean ± SEM obtained from three independent experiments (n = 3). Samples were compared using Student's t test. *$p < 0.05$; ns, not significant ($p > 0.05$).

(D) Expression of the *ADI* genes was measured via qRT-PCR upon treatment or removal of CHIR in mESCs. The data represent the mean ± SEM obtained from three independent experiments (n = 3). Samples were compared using Student's t test. *$p < 0.05$; **$p < 0.01$; ns, not significant ($p > 0.05$).

(E) Genomic tracks displaying long-range chromatin interactions obtained by Capture Hi-C (Joshi et al., 2015). First track: TCF7L1 ChIP-seq showing the TCF7L1 ChIP-seq peak, on the right of the *ADI* locus, marks the *ADI* enhancers. Second track: annotation of the *Aire*, *Dnmt3l*, and *Icosl* promoters. Third and fourth tracks: long-range chromatin interactions (serum and 2i, respectively) shown as arches connecting the associated regions. Relevant interactions whose anchor points (the *ADI* enhancer) overlap with *ADI* genes' promoters are annotated with thick red lines. For each of these tracks, the data correspond to two merged experimental replicates.

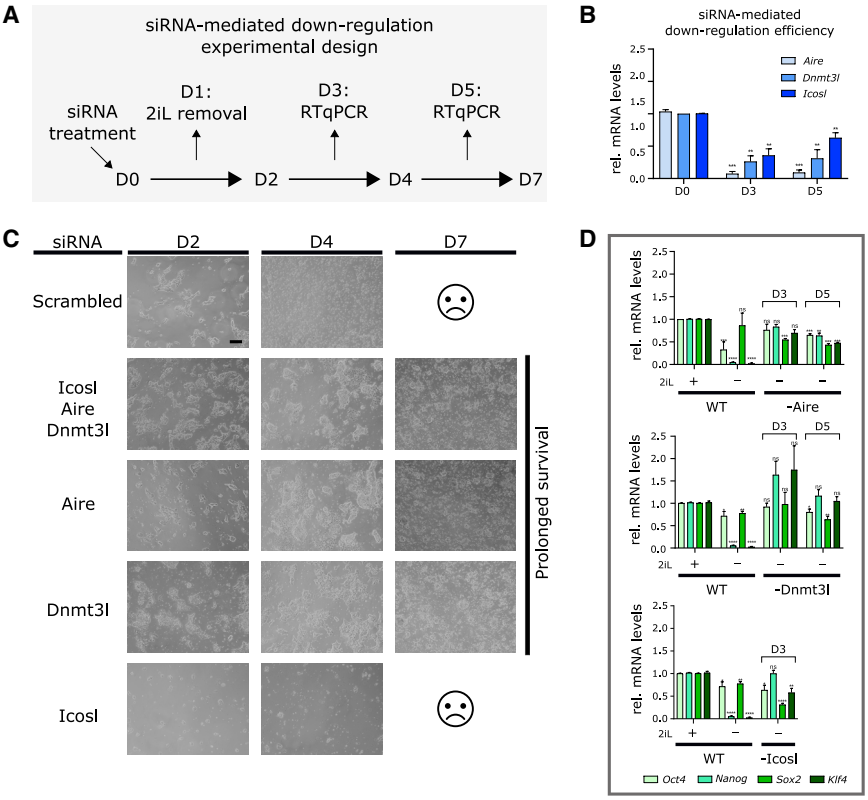

Figure 4. Knockdown of *ADI* renders mESCs 2iL independent

(A) Schematic description of siRNA-mediated downregulation of *ADI* genes

(B) Efficiency of downregulation of *Aire*, *Dnmt3b*, and *IcosL* measured by qRT-PCR performed on WT mESCs 3 and 5 days after specific siRNA treatment. The data represent the mean ± SEM obtained from three independent experiments (n = 3). Samples were compared using Student's t test. $^{**}p < 0.01$; $^{***}p < 0.001$.

(C) Cell viability after 7-day culture in N2B27 for scrambled siRNA-treated control mESCs or cells treated with specific *ADI* gene siRNAs. A black sad smile is used as placeholder for an otherwise empty plate as consequence of cell death. The black scale bar displayed on the top-left image represents approximately 200 μm.

(D) qRT-PCR analysis of *Oct4*, *Nanog*, *Sox2*, and *Klf4*, performed after siRNA treatment for each of the annotated gene (*Aire*, *Dnmt3L*, *IcosL*), cultured in N2B27 medium without 2iL. The data represent the mean ± SEM obtained from three independent experiments (n = 3). Samples were compared using Student's t test. $^{*}p < 0.05$; $^{**}p < 0.01$; $^{***}p < 0.001$; $^{****}p < 0.0001$; ns, not significant ($p > 0.05$).

to the possibility that their coordinated regulation and function might be a general phenomenon also important in other tissues.

Aire, *Dnmt3l*, and *IcosL* seem to be activated downstream of TCF/LEF and contribute to the balance between self-renewal and differentiation of mESCs. Of note, AIRE and DNMT3L have previously been implicated in mESC function. In line with the notion that AIRE could contribute to the exit of mESCs from the pluripotent state, knockdown of *Aire* in mESCs resulted in attenuated cell cycle but also in the reduction of differentiation-associated genes (Gu et al., 2010). DNMT3L, is an enzymatically inactive DNA methyltransferase that regulates enzymatically functional *de novo* methyltransferases DNMT3a and DNMT3b through direct protein-protein interactions (Suetake et al., 2004). DNMT3L was shown to function as regulator of DNA methylation in mESCs, and, consistent with our findings, its expression has been shown to decrease upon CHIR administration (Wu et al., 2013). The third gene, *IcosL*, encodes a secreted ligand that regulates B cell function (Liu et al., 2015); more work is needed to understand its yet-unknown role in mESCs. Intriguingly, *ICOSL* expression in cancer patients correlates with decreased survival, possibly indicating a function in sustained cell proliferation or self-renewal (Wang et al., 2019). Overall, our data support a model in which the *ADI* genes are activated by TCF7L1 and act as pro-differentiation factors.

Among different signaling pathways, Wnt/β-catenin has been shown to play a major role in the regulation of self-renewal and pluripotency of mESCs (Ogawa et al., 2006; Sato et al., 2004; Söderholm and Cantù, 2020). More specifically, Wnt/β-catenin signaling is required for the induction and patterning of endoderm and mesoderm during gastrulation, a process that can be mimicked *in vitro* in mESCs (Baillie-Johnson et al., 2015). Surprisingly, despite diverging functions of TCF/LEF members in mESCs (Lyashenko et al., 2011; Wray et al., 2011; Yi et al., 2011), a single TCF/LEF transcription factor has been shown to be capable of driving trilineage differentiation of mESCs (Moreira et al., 2017). Of note, the genes in the *ADI* locus that we identify in this work appear to be directly regulated by TCF7L1, in response to CHIR, but neither by TCF7 nor by β-catenin. Their expression is decreased when TCF/LEF are mutated but increases in response to CHIR removal. This is compatible with the notion that CHIR dampens the activation of *ADI* by TCF7L1, thereby contributing in sustaining the pluripotency network (Dunn et al., 2014). However, the *ADI* genes are unaffected by β-catenin deletion both in WT as well as in a qKO background. Consistent with this notion, no β-catenin was found to physically bind to the *ADI* locus. An intriguing possibility is that Plakoglobin/γ-catenin substitutes β-catenin in our βcatKO cells. γ-catenin has been shown to play a role for the activation of TCF/LEF target genes in β-catenin-deficient cells (Maeda et al., 2004). γ-catenin is also stabilized by CHIR, but its endogenous levels are not normally sufficient to promote the regulation of classic Wnt targets (Mahendram et al., 2013). While a possible regulation of the *ADI* locus by γ-catenin remains to be tested, we could not detect any upregulation of the *Jup* mRNA (encoding for γ-catenin) in our βcatKO cells (Figure S3F), that might hint at such a compensatory mechanism. Taken together, our data suggest that an alternative, β-catenin-independent but TCF/LEF-dependent regulatory mechanism is operating at the *ADI* locus in mESCs.

Limitations of the study

Our work leaves two questions unsolved. The first concerns the relevance of the interaction between TCF7L1 and the *ADI* enhancer, and how this is interrupted or attenuated by CHIR in a manner that likely does not involve β-catenin. Novel assays need to be employed to test the functional role of this physical association. For example, CRISPR/Cas-mediated deletion of the *ADI* enhancer, or mutation of the TCF7L1 binding motif contained in it, might impact TCF7L1 binding and the consequent regulation of *Aire*, *Dnmt3l*, and *IcosL*. Our model would predict that such genomic mutations would extend the lifespan of mESCs in the absence of 2iL.

Second, we did not address the mechanism by which the *ADI* genes contribute to the exit from the pluripotent state. Further loss-of-function and gain-of-function approaches in mESCs will be required to tackle this. In particular, whether *IcosL* contributes to this process at all remains unclear. It is plausible that the siRNA-mediated partial downregulation that we achieve is sufficient to affect pluripotency genes (Figures 4B and 4D) but not to extend renewal in the absence of 2iL (Figure 4C).

STAR★METHODS

Detailed methods are provided in the online version of this paper and include the following:

- KEY RESOURCES TABLE
- RESOURCE AVAILABILITY
  - Lead contact
  - Materials availability
  - Data and code availability
- EXPERIMENTAL MODEL AND SUBJECT DETAILS
  - Culture of cell lines
- METHOD DETAILS
  - Generation of knockout mESC lines
  - Embryoid body formation
  - Clonogenicity assays
  - Quantitative (q)RT-PCR
  - Western blot analyses
  - Antibodies
  - Electroporation
  - Transcriptomics analysis (RNA-seq)
  - Chromatin immunoprecipitation
- QUANTIFICATION AND STATISTICAL ANALYSIS
  - Statistical analysis
  - Western blot quantification
  - RNA-seq data analysis
  - β-catenin ChIP-seq data analysis

SUPPLEMENTAL INFORMATION

Supplemental information can be found online at https://doi.org/10.1016/j.celrep.2021.109705.

ACKNOWLEDGMENTS

This work was supported by the Swiss National Science Foundation and the Canton of Zurich to K.B., by the Knut and Alice Wallenberg Foundation, and by Cancerfonden to C.C. (CAN 2018/542) and the Canadian Institutes of Health Research to B.W.D. (MOP133610). The authors also thank the Functional Genomic Center of Zurich (FGCZ) for handling the RNA-seq libraries. The computations and data handling were enabled by resources provided by the Swedish National Infrastructure for Computing (SNIC) at [SNIC CENTRE] partially funded by the Swedish Research Council through grant agreement no. 2018-05973.

AUTHOR CONTRIBUTIONS

N.D., S.S., C.C., and K.B. designed the experiments. N.D. conducted the experiments and prepared the figure panels. S.S. performed the bioinformatics analyses and composed the figures. S.N. and B.W.D. generated the βcatKO and penKO cell clones. S.M. and B.W.D. performed ChIP-seq experiments of TCF7 and TCF7L1, and C.C. performed the ChIP-seq experiments of β-catenin. All authors assisted with data interpretation. C.C. and K.B. supervised the research teams and provided financial support for the study. C.C. wrote the manuscript with input from all authors. All authors contributed to multiple rounds of manuscript revision.

DECLARATION OF INTERESTS

The authors declare no competing interests.

Received: January 19, 2021
Revised: June 10, 2021
Accepted: August 23, 2021
Published: September 14, 2021

REFERENCES

Amemiya, H.M., Kundaje, A., and Boyle, A.P. (2019). The ENCODE Blacklist: Identification of Problematic Regions of the Genome. Sci. Rep. *9*, 9354.

Aulicino, F., Pedone, E., Sottile, F., Lluis, F., Marucci, L., and Cosma, M.P. (2020). Canonical Wnt Pathway Controls mESC Self-Renewal Through Inhibition of Spontaneous Differentiation via β-Catenin/TCF/LEF Functions. Stem Cell Reports *15*, 646–661.

Baillie-Johnson, P., van den Brink, S.C., Balayo, T., Turner, D.A., and Martinez Arias, A. (2015). Generation of aggregates of mouse embryonic stem cells that show symmetry breaking, polarization and emergent collective behaviour in vitro. J. Vis. Exp. *2015*, 1–10.

Benjamini, Y., and Hochberg, Y. (1995). Controlling the False Discovery Rate: A Practical and Powerful Approach to Multiple Testing. J. R. Stat. Soc. Ser. B *57*, 289–300.

Betschinger, J., Nichols, J., Dietmann, S., Corrin, P.D., Paddison, P.J., and Smith, A. (2013). Exit from pluripotency is gated by intracellular redistribution of the bHLH transcription factor Tfe3. Cell *153*, 335–347.

Blair, K., Wray, J., and Smith, A. (2011). The liberation of embryonic stem cells. PLoS Genet. *7*, e1002019.

Bonev, B., Mendelson Cohen, N., Szabo, Q., Fritsch, L., Papadopoulos, G.L., Lubling, Y., Xu, X., Lv, X., Hugnot, J.P., Tanay, A., and Cavalli, G. (2017). Multiscale 3D Genome Rewiring during Mouse Neural Development. Cell *171*, 557–572.

Chatterjee, S.S., Saj, A., Gocha, T., Murphy, M., Gonsalves, F.C., Zhang, X., Hayward, P., Akgöl Oksuz, B., Shen, S.S., Madar, A., et al. (2015). Inhibition of β-catenin-TCF1 interaction delays differentiation of mouse embryonic stem cells. J. Cell Biol. *211*, 39–51.

Chen, Y., Blair, K., and Smith, A. (2013). Robust self-renewal of rat embryonic stem cells requires fine-tuning of glycogen synthase kinase-3 inhibition. Stem Cell Reports *1*, 209–217.

Dixon, J.R., Selvaraj, S., Yue, F., Kim, A., Li, Y., Shen, Y., Hu, M., Liu, J.S., and Ren, B. (2012). Topological domains in mammalian genomes identified by analysis of chromatin interactions. Nature *485*, 376–380.

Dobin, A., Davis, C.A., Schlesinger, F., Drenkow, J., Zaleski, C., Jha, S., Batut, P., Chaisson, M., and Gingeras, T.R. (2013). STAR: ultrafast universal RNA-seq aligner. Bioinformatics *29*, 15–21.

Doetschman, T.C., Eistetter, H., Katz, M., Schmidt, W., and Kemler, R. (1985). The in vitro development of blastocyst-derived embryonic stem cell lines: formation of visceral yolk sac, blood islands and myocardium. J. Embryol. Exp. Morphol. *87*, 27–45.

Doumpas, N., Lampart, F., Robinson, M.D., Lentini, A., Nestor, C.E., Cantù, C., and Basler, K. (2019). TCF/LEF dependent and independent transcriptional regulation of Wnt/β-catenin target genes. EMBO J. *38*, e98873.

Dowen, J.M., Fan, Z.P., Hnisz, D., Ren, G., Abraham, B.J., Zhang, L.N., Weintraub, A.S., Schujiers, J., Lee, T.I., Zhao, K., and Young, R.A. (2014). Control of cell identity genes occurs in insulated neighborhoods in mammalian chromosomes. Cell *159*, 374–387.

Dunn, S.-J., Martello, G., Yordanov, B., Emmott, S., and Smith, A.G. (2014). Defining an essential transcription factor program for naïve pluripotency. Science *344*, 1156–1161.

Evans, M.J., and Kaufman, M.H. (1981). Establishment in culture of pluripotential cells from mouse embryos. Nature *292*, 154–156.

Ewels, P., Magnusson, M., Lundin, S., and Käller, M. (2016). MultiQC: summarize analysis results for multiple tools and samples in a single report. Bioinformatics *32*, 3047–3048.

Frankish, A., Diekhans, M., Ferreira, A.M., Johnson, R., Jungreis, I., Loveland, J., Mudge, J.M., Sisu, C., Wright, J., Armstrong, J., et al. (2019). GENCODE reference annotation for the human and mouse genomes. Nucleic Acids Res. *47* (*D1*), D766–D773.

Gu, B., Zhang, J., Chen, Q., Tao, B., Wang, W., Zhou, Y., Chen, L., Liu, Y., and Zhang, M. (2010). Aire regulates the expression of differentiation-associated genes and self-renewal of embryonic stem cells. Biochem. Biophys. Res. Commun. *394*, 418–423.

Guo, G., Huang, Y., Humphreys, P., Wang, X., and Smith, A. (2011). A PiggyBac-based recessive screening method to identify pluripotency regulators. PLoS ONE *6*, e18189.

Habib, S.J., Chen, B.C., Tsai, F.C., Anastassiadis, K., Meyer, T., Betzig, E., and Nusse, R. (2013). A localized Wnt signal orients asymmetric stem cell division in vitro. Science *339*, 1445–1448.

Huang, G., Ye, S., Zhou, X., Liu, D., and Ying, Q.L. (2015). Molecular basis of embryonic stem cell self-renewal: from signaling pathways to pluripotency network. Cell. Mol. Life Sci. *72*, 1741–1757.

Joshi, O., Wang, S.Y., Kuznetsova, T., Atlasi, Y., Peng, T., Fabre, P.J., Habibi, E., Shaik, J., Saeed, S., Handoko, L., et al. (2015). Dynamic Reorganization of Extremely Long-Range Promoter-Promoter Interactions between Two States of Pluripotency. Cell Stem Cell *17*, 748–757.

Kalkan, T., Bornelöv, S., Mulas, C., Diamanti, E., Lohoff, T., Ralser, M., Middelkamp, S., Lombard, P., Nichols, J., and Smith, A. (2019). Complementary Activity of ETV5, RBPJ, and TCF3 Drives Formative Transition from Naive Pluripotency. Cell Stem Cell *24*, 785–801.e7.

Kelly, K.F., Ng, D.Y., Jayakumaran, G., Wood, G.A., Koide, H., and Doble, B.W. (2011). β-catenin enhances Oct-4 activity and reinforces pluripotency through a TCF-independent mechanism. Cell Stem Cell *8*, 214–227.

Khan, A., and Mathelier, A. (2017). Intervene: a tool for intersection and visualization of multiple gene or genomic region sets. BMC Bioinformatics *18*, 287.

Kinoshita, M., Barber, M., Mansfield, W., Cui, Y., Spindlow, D., Stirparo, G.G., Dietmann, S., Nichols, J., and Smith, A. (2020). Capture of mouse and human stem cells with features of formative pluripotency. Cell Stem Cell *28*, 453–471.

Langmead, B., and Salzberg, S.L. (2012). Fast gapped-read alignment with Bowtie 2. Nat. Methods *9*, 357–359.

Li, H., Handsaker, B., Wysoker, A., Fennell, T., Ruan, J., Homer, N., Marth, G., Abecasis, G., and Durbin, R.; 1000 Genome Project Data Processing Subgroup (2009). The Sequence Alignment/Map format and SAMtools. Bioinformatics *25*, 2078–2079.

Li, M., Yu, J.S.L., Tilgner, K., Ong, S.H., Koike-Yusa, H., and Yusa, K. (2018). Genome-wide CRISPR-KO Screen Uncovers mTORC1-Mediated Gsk3 Regulation in Naive Pluripotency Maintenance and Dissolution. Cell Rep. *24*, 489–502.

Liu, D., Xu, H., Shih, C., Wan, Z., Ma, X., Ma, W., Luo, D., and Qi, H. (2015). T-B-cell entanglement and ICOSL-driven feed-forward regulation of germinal centre reaction. Nature *517*, 214–218.

Love, M.I., Huber, W., and Anders, S. (2014). Moderated estimation of fold change and dispersion for RNA-seq data with DESeq2. Genome Biol. *15*, 550.

Lyashenko, N., Winter, M., Migliorini, D., Biechele, T., Moon, R.T., and Hartmann, C. (2011). Differential requirement for the dual functions of β-catenin in embryonic stem cell self-renewal and germ layer formation. Nat. Cell Biol. *13*, 753–761.

MacDougall, M.S., Clarke, R., and Merrill, B.J. (2019). Intracellular Ca^{2+} Homeostasis and Nuclear Export Mediate Exit from Naive Pluripotency. Cell Stem Cell *25*, 210–224.e6.

Maeda, O., Usami, N., Kondo, M., Takahashi, M., Goto, H., Shimokata, K., Kusugami, K., and Sekido, Y. (2004). Plakoglobin (γ-catenin) has TCF/LEF family-dependent transcriptional activity in β-catenin-deficient cell line. Oncogene *23*, 964–972.

Mahendram, S., Kelly, K.F., Paez-Parent, S., Mahmood, S., Polena, E., Cooney, A.J., and Doble, B.W. (2013). Ectopic γ-catenin expression partially mimics the effects of stabilized β-catenin on embryonic stem cell differentiation. PLoS ONE *8*, e65320.

Martello, G., Sugimoto, T., Diamanti, E., Joshi, A., Hannah, R., Ohtsuka, S., Göttgens, B., Niwa, H., and Smith, A. (2012). Esrrb is a pivotal target of the Gsk3/Tcf3 axis regulating embryonic stem cell self-renewal. Cell Stem Cell *11*, 491–504.

Moreira, S., Polena, E., Gordon, V., Abdulla, S., Mahendram, S., Cao, J., Blais, A., Wood, G.A., Dvorkin-Gheva, A., and Doble, B.W. (2017). A Single TCF Transcription Factor, Regardless of Its Activation Capacity, Is Sufficient for Effective Trilineage Differentiation of ESCs. Cell Rep. *20*, 2424–2438.

Moreira, S., Seo, C., Polena, E., Mahendram, S., Mercier, E., Blais, A., and Doble, B.W. (2018). TCF7L1 and TCF7 differentially regulate specific mouse ES cell genes in response to GSK-3 inhibition. BioRxiv, 1–14.

Morgani, S., Nichols, J., and Hadjantonakis, A.K. (2017). The many faces of Pluripotency: in vitro adaptations of a continuum of in vivo states. BMC Dev. Biol. *17*, 7.

Mulas, C., Kalkan, T., von Meyenn, F., Leitch, H.G., Nichols, J., and Smith, A. (2019). Defined conditions for propagation and manipulation of mouse embryonic stem cells. Development *146*, dev173146.

Ogawa, K., Nishinakamura, R., Iwamatsu, Y., Shimosato, D., and Niwa, H. (2006). Synergistic action of Wnt and LIF in maintaining pluripotency of mouse ES cells. Biochem. Biophys. Res. Commun. *343*, 159–166.

Pereira, L., Yi, F., and Merrill, B.J. (2006). Repression of Nanog gene transcription by Tcf3 limits embryonic stem cell self-renewal. Mol. Cell. Biol. *26*, 7479–7491.

Qiu, D., Ye, S., Ruiz, B., Zhou, X., Liu, D., Zhang, Q., and Ying, Q.L. (2015). Klf2 and Tfcp2l1, Two Wnt/β-Catenin Targets, Act Synergistically to Induce and Maintain Naive Pluripotency. Stem Cell Reports *5*, 314–322.

Quinlan, A.R., and Hall, I.M. (2010). BEDTools: a flexible suite of utilities for comparing genomic features. Bioinformatics *26*, 841–842.

Ritchie, M.E., Phipson, B., Wu, D., Hu, Y., Law, C.W., Shi, W., and Smyth, G.K. (2015). limma powers differential expression analyses for RNA-sequencing and microarray studies. Nucleic Acids Res. *43*, e47.

Robinson, J.T., Thorvaldsdóttir, H., Winckler, W., Guttman, M., Lander, E.S., Getz, G., and Mesirov, J.P. (2011). Integrative genomics viewer. Nat. Biotechnol. *29*, 24–26.

Sato, N., Meijer, L., Skaltsounis, L., Greengard, P., and Brivanlou, A.H. (2004). Maintenance of pluripotency in human and mouse embryonic stem cells through activation of Wnt signaling by a pharmacological GSK-3-specific inhibitor. Nat. Med. *10*, 55–63.

Schneider, C.A., Rasband, W.S., and Eliceiri, K.W. (2012). NIH Image to ImageJ: 25 years of image analysis. Nat. Methods *9*, 671–675.

Smith, A.G., Heath, J.K., Donaldson, D.D., Wong, G.G., Moreau, J., Stahl, M., and Rogers, D. (1988). Inhibition of pluripotential embryonic stem cell differentiation by purified polypeptides. Nature *336*, 688–690.

Söderholm, S., and Cantù, C. (2020). The WNT/β-catenin dependent transcription: A tissue-specific business. Wiley Interdiscip. Rev. Syst. Biol. Med. Published online October 21, 2020. https://doi.org/10.1002/wsbm.1511.

Štefková, K., Procházková, J., and Pacherník, J. (2015). Alkaline phosphatase in stem cells. Stem Cells Int. *2015*, 628368.

Suetake, I., Shinozaki, F., Miyagawa, J., Takeshima, H., and Tajima, S. (2004). DNMT3L stimulates the DNA methylation activity of Dnmt3a and Dnmt3b through a direct interaction. J. Biol. Chem. *279*, 27816–27823.

Supek, F., Bošnjak, M., Škunca, N., and Šmuc, T. (2011). REVIGO summarizes and visualizes long lists of gene ontology terms. PLoS ONE *6*, e21800.

Villegas, F., Lehalle, D., Mayer, D., Rittirsch, M., Stadler, M.B., Zinner, M., Olivieri, D., Vabres, P., Duplomb-Jego, L., De Bont, E.S.J.M., et al. (2019). Lysosomal Signaling Licenses Embryonic Stem Cell Differentiation via Inactivation of Tfe3. Cell Stem Cell *24*, 257–270.

Wang, Y., Song, F., Zhang, B., Zhang, L., Xu, J., Kuang, D., Li, D., Choudhary, M.N.K., Li, Y., Hu, M., et al. (2018). The 3D Genome Browser: a web-based browser for visualizing 3D genome organization and long-range chromatin interactions. Genome Biol. *19*, 151.

Wang, B., Jiang, H., Zhou, T., Ma, N., Liu, W., Wang, Y., and Zuo, L. (2019). Expression of ICOSL is associated with decreased survival in invasive breast cancer. PeerJ *7*, e6903.

Wickham, H. (2016). ggplot2: Elegant Graphics for Data Analysis (New York: Springer-Verlag), ISBN 978-3-319-24277-4. https://ggplot2.tidyverse.org.

Wray, J., Kalkan, T., Gomez-Lopez, S., Eckardt, D., Cook, A., Kemler, R., and Smith, A. (2011). Inhibition of glycogen synthase kinase-3 alleviates Tcf3 repression of the pluripotency network and increases embryonic stem cell resistance to differentiation. Nat. Cell Biol. *13*, 838–845.

Wu, Y., Ai, Z., Yao, K., Cao, L., Du, J., Shi, X., Guo, Z., and Zhang, Y. (2013). CHIR99021 promotes self-renewal of mouse embryonic stem cells by modulation of protein-encoding gene and long intergenic non-coding RNA expression. Exp. Cell Res. *319*, 2684–2699.

Ye, S., Zhang, T., Tong, C., Zhou, X., He, K., Ban, Q., Liu, D., and Ying, Q.L. (2017). Depletion of *Tcf3* and *Lef1* maintains mouse embryonic stem cell self-renewal. Biol. Open *6*, 511–517.

Yeo, J.C., Jiang, J., Tan, Z.Y., Yim, G.R., Ng, J.H., Göke, J., Kraus, P., Liang, H., Gonzales, K.A.U., Chong, H.C., et al. (2014). Klf2 is an essential factor that sustains ground state pluripotency. Cell Stem Cell *14*, 864–872.

Yi, F., Pereira, L., Hoffman, J.A., Shy, B.R., Yuen, C.M., Liu, D.R., and Merrill, B.J. (2011). Opposing effects of Tcf3 and Tcf1 control Wnt stimulation of embryonic stem cell self-renewal. Nat. Cell Biol. *13*, 762–770.

Ying, Q.L., Wray, J., Nichols, J., Batlle-Morera, L., Doble, B., Woodgett, J., Cohen, P., and Smith, A. (2008). The ground state of embryonic stem cell self-renewal. Nature *453*, 519–523.

Yu, G., Wang, L.G., and He, Q.Y. (2015). ChIPseeker: an R/Bioconductor package for ChIP peak annotation, comparison and visualization. Bioinformatics *31*, 2382–2383.

Zhang, Y., Liu, T., Meyer, C.A., Eeckhoute, J., Johnson, D.S., Bernstein, B.E., Nusbaum, C., Myers, R.M., Brown, M., Li, W., and Liu, X.S. (2008). Model-based analysis of ChIP-Seq (MACS). Genome Biol. *9*, R137.

Zhu, L.J., Gazin, C., Lawson, N.D., Pagès, H., Lin, S.M., Lapointe, D.S., and Green, M.R. (2010). ChIPpeakAnno: a Bioconductor package to annotate ChIP-seq and ChIP-chip data. BMC Bioinformatics *11*, 237.

STAR★METHODS

KEY RESOURCES TABLE

Reagent or resource	Source	Identifier
Antibodies		
α-tubulin	Sigma-Aldrich	Cat# T6074; RRID:AB_477582
TCF7	Cell Signaling	Cat# C63D9; RRID:AB_2199302
LEF1	Cell Signaling	Cat# C12A5; RRID:AB_823558
TCF7L1	Abcam	Cat# ab86175; RRID:AB_1925494
TCF7L2	Cell Signaling	Cat# C48H11; RRID:AB_2199816
β-catenin	R&D system	Cat# AF1329; RRID:AB_354736
β-catenin	Santa Cruz	Cat# SC-7963; RRID:AB_626807
HRP anti-mouse	Jackson	Cat# 115-035-003; RRID:AB_10015289
HRP anti-rabbit	Jackson	Cat# 111-035-144; RRID:AB_2307391
Bacterial and virus strains		
DH5a Competent Cells	ThermoFisher (eBioscience)	Cat# 18265017
Chemicals, peptides, and recombinant proteins		
DMEM (1X) + GlutaMAX	GIBCO	31966-021
DMEM (1x)	GIBCO	41966-029
Opti-MEM	GIBCO	31985062
Heat Inactivated FBS	GIBCO	10500-064
TrypLE Express	GIBCO	12604-013
Trypsin-EDTA	GIBCO	25200056
Tween 20	Sigma	P1379-250ML
PBS, pH 7.4 (1X)	GIBCO	10010-015
Tris(hydroxymethyl)aminomethane	Biosolve	200923
Triton X-100	Sigma-Aldrich	93443
SDS	Sigma-Aldrich	11667289001
HEPES	Millipore	391340
EDTA	Sigma-Aldrich	93283
EGTA	Millipore	324626
Pen/strep	ThermoFischer	15140-122
B27 (50x)	ThermoFischer	17504-044
N2 (100x)	ThermoFischer	17502-048
Gelatine	Sigma-Aldrich	G1890
CHIR99021	STEMCELL technologies	72052
PD0325901	STEMCELL technologies	72184
ESGRO	Merck	ESG1107
Puromycin	Sigma-Aldrich	P8833-10MG
SYBR Green SuperMix	BioRad	170880
Bovine Serum Albumin Fraction V	Sigma	10735086001
ethylene glycol-bis	Merck	E3257-250MG
Laminin	Sigma-Aldrich	L2020
NuPAGE	ThermoFischer	NP0004
formaldehyde	Sigma-Aldrich	47608-1L-F
Critical commercial assays		
AP kit	Sigma-Aldrich	SCR004
Lipofectamine® 3000	ThermoFischer	L3000001

(*Continued on next page*)

Continued

Reagent or resource	Source	Identifier
FuGENE® HD Transfection Reagent	Promega	E2311
PureLink RNA Mini Kit	ThermoFischer	12183020
High Fidelity cDNA Synthesis Kit	Roche	05081955001
Dual-Luciferase Reporter Assay System	Promega	E1910
DNA-free	ThermoFischer	AM1906
Deposited data		
Raw and processed RNA-seq data	This paper	ArrayExpress: E-MTAB-10564
Raw and processed ChIP-seq data (β-catenin)	This paper	ArrayExpress: E-MTAB-10575
ChIA-PET data	Dowen et al., 2014	GEO: GSE57913
Capture Hi-C data	Joshi et al., 2015	GEO: GSE72164
Mouse reference genome and annotation, release M24, GENCODE	Frankish et al., 2019	https://www.gencodegenes.org/mouse/
Mouse reference genome GRCm38/ mm10), UCSC	UCSC	http://hgdownload.cse.ucsc.edu/ goldenpath/mm10/bigZips/
ENCODE blacklisted regions, v.2	Amemiya et al., 2019	https://github.com/Boyle-Lab/Blacklist/ tree/master/lists
UCSC liftOver chain data, mm9 to mm10	UCSC	http://hgdownload.soe.ucsc.edu/ goldenPath/mm9/liftOver/mm9ToMm10. over.chain.gz
Experimental models: Cell lines		
HEK293T	ATTC	CRL-3216
E14TG2a	ATTC	CRL-182
Oligonucleotides		
PCR primers and guide RNAs designed in this study	See Table S4 for oligonucleotide information	N/A
Software and algorithms		
ImageJ (FIJI) v. 2.0.0	Schneider et al., 2012	https://imagej.net/software/imagej/
Prism 9	Graphpad	https://www.graphpad.com/ scientific-software/prism/
R programming language, v. 3.4.4	R Core Team, 2017	https://www.r-project.org/
Rstudio, v. 1.1.463	Rstudio Team, 2020	https://www.rstudio.com/
FastQC, v. 0.11.5	Babraham Bioinformatics, Babraham Institute	https://anaconda.org/bioconda/fastqc
MultiQC, v. 1.7	Ewels et al., 2016	https://anaconda.org/bioconda/multiqc
SamTools, v. 1.9	Li et al., 2009	https://anaconda.org/bioconda/samtools
BedTools, v. 2.26.0	Quinlan and Hall, 2010	https://anaconda.org/bioconda/bedtools
ggplot2, R-package, v. 3.2.1	(Wickham, 2016)	https://ggplot2.tidyverse.org/
Integrative Genomic Viewer (IGV), v. 2.4.17	Robinson et al., 2011	https://anaconda.org/bioconda/igv
BBDuk, part of the BBTools suite, v. 38.58	Bushnell, n.d.	https://sourceforge.net/projects/bbmap
Spliced Transcripts Alignment to a Reference (STAR), v. 2.7.3a	Dobin et al., 2013	https://anaconda.org/bioconda/star
DESeq2, R-package, v. 1.18.1	Love et al., 2014	https://bioconductor.org/packages/3.6/ bioc/html/DESeq2.html
Limma, R-package, v. 3.34.9	Ritchie et al., 2015	https://bioconductor.org/packages/3.6/ bioc/html/limma.html
Benjamini-Hochberg FDR correction (DESeq2)	Benjamini and Hochberg, 1995	http://www.math.tau.ac.il/~ybenja/ MyPapers/benjamini_hochberg1995.pdf
REVIGO	Supek et al., 2011	http://revigo.irb.hr/
Bowtie2, v. 2.3.4.1	Langmead and Salzberg, 2012	https://anaconda.org/bioconda/bowtie2
MACS2, v. 2.2.6	Zhang et al., 2008	https://anaconda.org/bioconda/macs2

(*Continued on next page*)

Continued

Reagent or resource	Source	Identifier
ChIPpeakAnno, R-package, v. 3.12.7	Zhu et al., 2010	https://www.bioconductor.org/packages/3.6/bioc/html/ChIPpeakAnno.html
ChIPseeker, R-package, v. 1.14.2	Yu et al., 2015	https://www.bioconductor.org/packages/3.6/bioc/html/ChIPseeker.html
Intervene, v. 0.6.4	Khan and Mathelier, 2017	https://anaconda.org/bioconda/intervene
3D Genome Browser	Wang et al., 2018	http://3dgenome.fsm.northwestern.edu/

RESOURCE AVAILABILITY

Lead contact

Further information and requests for resources and reagents should be directed to and will be fulfilled by the Lead Contact, Claudio Cantù (claudio.cantu@liu.se).

Materials availability

All newly generated plasmids and cell lines in this study are available by contacting the lead contact.

Data and code availability

The RNA-seq and ChIP-seq datasets generated during this study have been deposited at the ArrayExpress Archive of Functional Genomic Data and are publicly available as of the date of this publication. Dataset accession numbers are listed in the key resources table (ArrayExpress: E-MTAB-10564, E-MTAB-10575). Microscopy and quantitative (q)RT-PCR data reported in this paper are shared by the lead contact upon request.

This study did not generate any novel software or algorithms. Published and freely available software and algorithms used for analysis in this study are listed in the key resources table. Original codes are shared by the lead contact upon request.

Any additional information required to reanalyze the data reported in this paper is available from the lead contact upon request.

EXPERIMENTAL MODEL AND SUBJECT DETAILS

Culture of cell lines

E14TG2a (ATTC CRL-182) mESCs were obtained from Doble lab. mESCs were cultured in media containing N2B27 (GIBCO) supplemented with 2i/LIF, unless otherwise indicated, at the following final concentrations: PD0325901 (MEKi, Stem Cell), 1 μM; CHIR99021 (GSK3i, Stem Cell), 3 μM; LIF (Millipore), 1:1000.

For passaging, cells were dissociated with TrypLE express (GIBCO) for 3′, pelleted by centrifugation (250 g), and resuspended in fresh 2i/LIF. mESCs were maintained in filtered T25 flasks (TPP) coated with 0.1% Gelatine (Sigma-Aldrich, G1890). Cells were passaged every 2 days.

Human embryonic kidney 293 cells were cultured in media consisting of DMEM, high glucose (41966-029 GIBCO) supplemented with 10% fetal bovine serum (GIBCO), 1x penicillin-streptomycin according to the manufacturer's recommendation.

METHOD DETAILS

Generation of knockout mESC lines

Knockout cell lines were created using pSpCas9-PX459 V2.0 plasmid. 200,000 cells were transfected using Lipofectamine® 2000 DNA Transfection Reagent protocol (Invitrogen). After 24 hours, cells were subjected to 2 μM puromycin to kill untransfected lacking puromycin resistance conferred by the vector. Puromycin selection was only maintained for 24 hours after which cells were allowed to grow in standard medium until single colonies were visible. Single colonies were isolated and allowed to expand.

Embryoid body formation

To differentiate cells to embryoid bodies (EB), cells were suspended in N2B27 medium supplemented with 2i without LIF and 10% of Fetal Bovine Serum (hereafter referred to as EB medium). Droplets of cells, each containing 800 mESCs / 30 μL EB medium were plated on the lid of 10 cm^2 Petri dishes. The Petri dishes were placed in incubator (37°C, 5% CO_2) for 3 days. Each droplet was then transferred to ultra-low adhesion 96-well plate, containing 200 μL of EB medium. The EB medium was replenished every two days.

Clonogenicity assays

For clonogenicity assays, cells were dissociated at 40-48h post-2i withdrawal, and following resuspension in appropriate media. Cells were plated at single cell density (500 cells / 6-well) in 2i/LIF or N2B27 on plates coated with 1% Laminin (Sigma, Cat.

L2020) in triplicate. At day 6, alkaline phosphatase staining was performed using an AP Kit (Sigma-Aldrich). Colonies were scored manually.

Quantitative (q)RT-PCR

Total RNA (1 μg) isolated using the PureLink RNA Mini Kit (Thermo Fisher Scientific) was used to generate cDNA with Transcription High Fidelity cDNA Synthesis Kit (Roche) and then treated with DNA-free Kit (Thermo Fisher Scientific). SYBR Green SuperMix (Bio-Rad) was used for qPCR reactions using 3 μL of diluted cDNA (1 μg RNA equivalent in 100 μL). GAPDH was used as the reference gene. QuantStudio 3 (Thermo Fisher Scientific) instrument and software were used to determine relative gene expression levels using the delta-delta Ct method. Primer sequences were designed using Roche's online primer design software (https://lifescience.roche.com/en_ch/brands/universal-probe-library.html) or were obtained from prior publications (Table S4). Statistical analyses (two-tailed Student's t test) were performed in Microsoft Excel considering both independent experiments and technical repetitions. Each experiment was performed at least three times.

Western blot analyses

Cell lysates were mixed with LDS sample buffer supplemented with Sample Reducing Agent (Invitrogen) and heated for 5′ at 95C. 10–15 μg of protein/lane was run through 10% Bis-Tris gels (120V, 90'). Proteins were transferred onto polyvinylidene fluoride (PVDF) membranes with a Bio-Rad Mini Trans-Blot System (35V,3h). Membranes were blocked with 5% milk/PBS-T (Phosphate-buffered saline supplemented with tween 20) for 45' in room temperature (RT) and incubated with primary antibodies diluted in 5% Bovine Serum Albumin/PBS-T overnight at 4C. Blots were washed with PBS-T (four times, 15'/wash), and incubated with horseradish peroxidase (HRP)-conjugated secondary antibodies (1hr, RT). After four washes with 15' in PBS-T, blots were incubated in WesternBright Quantum (Advansta) and imaged by using a Fusion SL imaging System (Vilmer).

Antibodies

The following primary antibodies were used for western blots: mouse anti-α-tubulin (T6074, Sigma-Aldrich), rabbit anti-TCF7 (C63D9, Cell Signaling), rabbit anti-LEF1 (C12A5, Cell Signaling), rabbit anti-TCF7L1 (ab86175, Abcam), rabbit anti-TCF7L2 (C48H11, Cell Signaling), mouse anti-β-catenin (AF1329: R&D system); mouse anti-β-catenin carboxy (SC-7963: Santa Cruz). Horseradish peroxidase-conjugated secondary anti-mouse and anti-rabbit antibodies for western blotting were purchased from Jackson.

Electroporation

mESCs were collected in a 15 mL tube and pelleted at 145 g for 5′. For each electroporation experiment, the cell pellet was resuspended in Opti-MEM medium to a final concentration of 10^6 cells per 100 μL. The corresponding siRNAs (Sigma-Aldrich) in 300 nM final were added to the cell mix.

For the electroporation a NEPA electroporator was used with the following set up; poring pulse: 135(V), 5(ms), 50(ms), 10(D.rate) + (polarity); transfer pulse: 20(V), 50(ms), 59(ms), 40(D.ate)+-(polarity).

After the cells were electroporated, they were transferred to a 12-well plate supplemented with 1 mL of the appropriate cell medium and monitored for at least 8 days.

Transcriptomics analysis (RNA-seq)

Library preparation and sequencing was performed by the Functional Genomics Center Zurich (FGCZ), Switzerland. Quality of isolated RNA was determined with a Qubit® (1.0) Fluorometer (Life Technologies, California, USA) and a Fragment Analyzer (Agilent, Santa Clara, California, USA). Only those samples with a 260 nm/280 nm ratio between 1.8–2.1 and a 28S/18S ratio within 1.5–2 were further processed. The TruSeq Stranded mRNA (Illumina, Inc, California, USA) was used in the succeeding steps. Briefly, total RNA samples (100-1000 ng) were polyA enriched and then reverse-transcribed into double-stranded cDNA. The cDNA samples were fragmented, end-repaired and adenylated before ligation of TruSeq adapters containing unique dual indices (UDI) for multiplexing. Fragments containing TruSeq adapters on both ends were selectively enriched with PCR. The quality and quantity of the enriched libraries were validated using Qubit® (1.0) Fluorometer and the Fragment Analyzer (Agilent, Santa Clara, California, USA). The product is a smear with an average fragment size of approximately 260 bp. The libraries were normalized to 10nM in Tris-Cl 10 mM, pH8.5 with 0.1% Tween 20. The Novaseq 6000 (Illumina, Inc, California, USA) was used for cluster generation and sequencing according to standard protocol. Sequencing was single end at 100 bp. The RNA-seq datasets (raw and processed files) have been deposited at ArrayExpress under accession number E-MTAB-10564.

Chromatin immunoprecipitation

β-catenin ChIP on mESC was performed using previous procedures and antibodies as described before for HEK293T (Doumpas et al., 2019). Briefly, mESC were treated with increased CHIR up to 10 μM for 24 h to stimulated Wnt/β-catenin signaling. Ca. 10×10^6 cells per samples were cross-linked in 20 mL PBS for 40' with the addition of 1.5 mM ethylene glycol-bis(succinimidyl succinate) (Thermo Scientific, Waltham, MA, USA), for protein–protein cross-linking, and 1% formaldehyde for the last 20' of incubation, to preserve DNA–protein interactions. The reaction was blocked with glycine and the cells were subsequently lysed in 1 mL HEPES buffer (0.3% SDS, 1% Triton X-100, 0.15 M NaCl, 1 mM EDTA, 0.5 mM EGTA, 20 mM HEPES). Chromatin was sheared using Covaris

S2 (Covaris, Woburn, MA, USA) for 8' with the following set up: duty cycle: max, intensity: max, cycles/burst: max, mode: Power Tracking. The sonicated chromatin was diluted to 0.15% SDS and incubated overnight at 4°C with 10 μg of anti-β-catenin (SantaCruz sc-7199 or Cell Signaling) and 50 μL of protein A/G magnetic beads (Upstate). The beads were washed at 4°C with wash buffer 1 (0.1% SDS, 0.1% deoxycholate, 1% Triton X-100, 0.15 M NaCl, 1 mM EDTA, 0.5 mM EGTA, 20 mM HEPES), wash buffer 2 (0.1% SDS, 0.1% sodium deoxycholate, 1% Triton X-100, 0.5 M NaCl, 1 mM EDTA, 0.5 mM EGTA, 20 mM HEPES), wash buffer 3 (0.25 M LiCl, 0.5% sodium deoxycholate, 0.5% NP-40, 1 mM EDTA, 0.5 mM EGTA, 20 mM HEPES) and finally twice with Tris EDTA buffer. The chromatin was eluted with 1% SDS, 0.1 M $NaHCO_3$, de-cross-linked by incubation at 65°C for 5 h with 200 mM NaCl, extracted with phenol–chloroform and ethanol-precipitated. The immunoprecipitated DNA was used as input material for DNA deep sequencing.

QUANTIFICATION AND STATISTICAL ANALYSIS

Statistical analysis

Statistical analysis was performed in Prism v9. Statistical details for all experiments, including value and definition of n, error bars, and significance thresholds can be found in the Figure Legends.

Western blot quantification

TCF7L1 protein abundance in WT and βcatKO cell lines was quantified using the image analysis software ImageJ (version 1.52n). Integrated density was measured for the TCF7L1 band in each lane and divided by the value of the corresponding Tubulin band. Each lane was normalized to the first land (WT no CHIR) giving relative integrated density values.

RNA-seq data analysis

Raw data in the form of obtained fastq files were controlled for sequencing quality using the tool FastQC (0.11.5). Sequencing reads were trimmed to remove adaptor remnants using BBDuk, part of the BBTools suite (38.58). MultiQC (1.7) (Ewels et al., 2016) was used to summarize the quality results.

Mouse mm10 reference genome and corresponding annotation data were downloaded from GENCODE, release M24 (https://www.gencodegenes.org/mouse/) to which pre-processed sequenced reads were mapped using the Spliced Transcript Alignment to a Reference (STAR) software (2.7.3a) (Dobin et al., 2013) with –quantMode TranscriptomeSAM GeneCounts settings.

Downstream analysis, annotation and visualization was made with the R programming language and Rstudio. Differential gene expression analysis was performed using DESeq2 (1.18.1) (Love et al., 2014) and obtained p values were adjusted for multiple comparisons through the Benjamini-Hochberg false discovery rate (FDR) procedure (Benjamini and Hochberg, 1995). An FDR adjusted p value below 0.05 was used as cut-off when determining statistical significance. Functional enrichment analysis of differentially expressed genes (DEGs) was performed using the goana function in the limma package (3.34.9) (Ritchie et al., 2015), based on gene function information from the Gene Ontology (GO) knowledgebase. Obtained significant GO terms ($p < 0.05$) were further filtered by removing redundant GO terms based on semantic similarity (simRel score ≤ 0.7) using the online tool REVIGO (Supek et al., 2011).

β-catenin ChIP-seq data analysis

Raw sequencing data were quality checked using FastQC (0.11.5). Because all the samples showed high average phred quality scores > 30 and no detected sequencing adaptor remnants, no trimming step was deemed necessary. Reads were then mapped to the mouse reference genome (version GRCm38) by end-to-end alignment using the read alignment tool Bowtie2 (2.3.4.1) (Langmead and Salzberg, 2012). Aligned reads were sorted and indexed using samtools (1.9) (Li et al., 2009) and reads mapped to the mitochondrial chromosome were removed. Genomic enrichment of aligned reads was determined with the peak calling tool MACS2 (2.2.6) (Zhang et al., 2008), using the penta knockout sample as control. Finally, peaks within ENCODE blacklisted regions were removed using BedTools (2.26.0) (Quinlan and Hall, 2010). Overlap between called peaks in replicates was determined with Intervene (0.6.4) (Khan and Mathelier, 2017), a tool for intersection of genomic regions, and used as basis for the definition of consensus peak sets. Visualization of aligned read enrichment as genomic tracks was produced using the Integrative Genomics Viewer (IGV) (2.4.17) (Robinson et al., 2011).